01 Jan 2005

Image Quality vs. NEC in 2D and 3D PET

John W. Wilson
Missouri University of Science and Technology, jwilson@mst.edu

Timothy G. Turkington

Josh M. Wilson

James G. Colsher

et. al. For a complete list of authors, see https://scholarsmine.mst.edu/min_nuceng_facwork/1201

Recommended Citation

J. W. Wilson et al., "Image Quality vs. NEC in 2D and 3D PET," *IEEE Nuclear Science Symposium Conference Record, 2005*, Institute of Electrical and Electronics Engineers (IEEE), Jan 2005.
The definitive version is available at https://doi.org/10.1109/NSSMIC.2005.1596756

Image Quality vs. NEC in 2D and 3D PET

John W. Wilson, Timothy G. Turkington, *Member, IEEE,* Josh M. Wilson, James G. Colsher, *Member, IEEE*, Steven G. Ross, *Member, IEEE*.

***Abstract*–To investigate the relationship between NEC and image quality in 2D and 3D PET, while simultaneously optimizing 3D low energy threshold (LET), we have performed a series of phantom measurements. The phantom consisted of 46 1 cm fillable hollow spheres on a random grid inside a water-filled oval cylinder, 21 cm tall, 36 cm wide, and 40 cm long. The phantom was imaged on a Discovery ST PET/CT system (GE Healthcare, Milwaukee, WI) in a series of 3 min scans as it decayed from an activity of 7.2 mCi. The scans included LET settings of 375, 400, and 425 keV in 3D, and 375 keV in 2D. Image signal-to-noise (SNR) was calculated and compared with NEC. While both NEC and image quality in 3D improved for LETs above the default of 375 keV, we found that there were significant differences between NEC and image quality for 2D and 3D. Most importantly, 3D image-quality was strongly dependent on the reconstruction algorithm and its associated parameters. In conclusion, a direct measure of image quality is necessary for comparing 2D vs. 3D performance.**

I. Introduction

COMPARISON of 2D and 3D imaging modes in PET has often been based on count statistics, specifically, the noise equivalent counts (NEC) [1]. While such comparisons are a useful starting point, important factors, such as different spatial resolutions and the inherently different reconstruction methods that must be used for 2D vs. 3D data, limit the utility of comparisons based on NEC alone. Image quality measures [2],[3] that reflect not only raw data count statistics but spatial resolution, image reconstruction, and other image-degrading factors, provide a more useful basis for comparison, but can be challenging to perform.

An additional factor to consider is that each modality (2D and 3D) must be optimized on its own, including level of radioactivity and acquisition parameters such as the low energy threshold. Raising the low energy threshold (LET) in PET decreases the number of scattered photons detected by the system. This lowers both the scatter fraction and the random rate, at the expense of decreased sensitivity. With high scatter fractions, changes to the LET can have significant impact on 3D PET performance [4].

Previous line source measurements [4] have shown that raising the LET on a GE Discovery ST from its default of 375 keV improves NEC for a variety of phantom sizes when scanning in 3D mode.

To investigate the relationship between NEC and image quality in comparing 2D and 3D PET, while simultaneously optimizing the LET for 3D PET, we have performed a series of phantom measurements using a novel image-quality phantom [5] that emulates an average patient size [6] and uses many small radioactive spheres.

II. Methods and Results

A. Phantom

All scans were performed on a Discovery ST PET/CT system (GE Healthcare, Milwaukee, WI) [7]. The phantom consisted of 46 1-cm fillable hollow plastic spheres mounted on a rectangular grid in x and y, but at random locations in the axial direction over a range of ~4 cm. The spheres were inside a water-filled oval cylinder, 21 cm tall, 36 cm wide, and 40 cm long. (Fig. 1).

For this phantom, we estimate that equivalent patient injected dose is equal to 4.4 times the total phantom radioactivity (including FDG distribution considerations and a decay from a 45 min FDG uptake period). The phantom was filled with a total radioactivity of 7.2 mCi (corresponding to an injection patient dose of 31.7 mCi), with a sphere-to-background activity ratio of 4 to 1. Additionally, the spheres contained a 2.5% solution of Gastrografin (Iodine-based CT contrast agent), which allowed the sphere locations to be easily identified on the corresponding CT image. The phantom was imaged in a series of 3 min scans as it decayed over 5 half-lives. The scans alternated between LET values of 375, 400, and 425 keV in 3D mode, and 2D at 375 keV. Images were reconstructed into a 50 cm field of view on a matrix size of 128x128 pixels, with CT-based attenuation correction, and delayed-events based randoms correction

Manuscript received November 11, 2005. Work supported in part by GE Healthcare Technologies.

J. W. Wilson is with Department of Radiology of Duke University Medical Center, Durham, NC 27710 USA (telephone: 919-684-7978, e-mail: jwwilson@petsparc.mc.duke.edu).

T. G. Turkington is with Department of Radiology of Duke University Medical Center, Durham, NC 27710 USA (telephone: 919-684-7706, e-mail: timothy.turkington@duke.edu).

J. M. Wilson is with Department of Radiology of Duke University Medical Center, Durham, NC 27710 USA.

J. G. Colsher is with GE Healthcare Technologies, Milwaukee, WI (telephone: 919-401-8607, e-mail: james.colsher@med.ge.com).

S. G. Ross is with GE Healthcare Technologies, Milwaukee, WI (e-mail: steven.ross@med.ge.com).

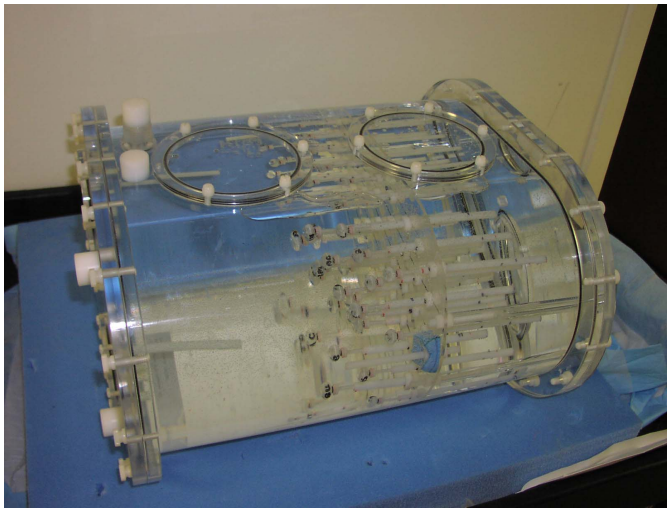

Fig. 1: Phantom with insert.

B. Calculating NEC.

To calculate NEC, the total scan prompts (P) and total delayed events (D) were acquired for each scan. True events (T) were derived from (P-D) using the fraction of true-to-scattered events as measured using a line source in the same phantom. Scattered events (S) were similarly derived from P-D using line source measurements, but using the ratio of scattered events *within the phantom body* to true events as only these contribute to image noise. Using T, S and R, the NEC was calculated for each scan in the decay series as

$$\frac{T}{1+S/T+2(0.48)R/T} \qquad (1)$$

where the factor of 0.48 accounts for the fraction of random counts inside the phantom body, and the factor of 2 accounts for delayed events based randoms correction. The NEC results for the four different scan types are shown below. This measure of NEC agrees well with previously published line source based measurements [4].

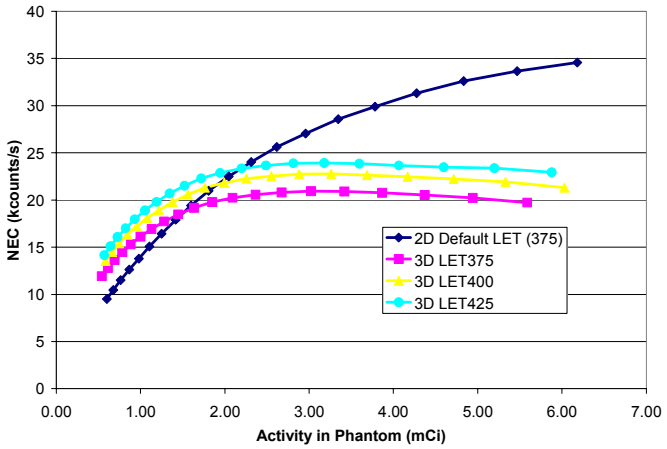

Fig. 2: NEC vs. activity for the whole body phantom with image quality insert.

C. Calculating signal to noise ratio.

To calculate image signal to noise ratio (SNR), an automated program was used to define the sphere ROIs on the contrast-enhanced CT. The program also defined 6 background ROIs in the vicinity of each signal sphere. Sphere and background ROIs were then applied to the PET images, using the known registration between the two, but applying a small shift in x, y, and z, based on maximizing the PET intensities at the CT sphere locations, to account for any inaccuracy in alignment between PET and CT images. For each sphere *i*, signal and background ROI mean values were extracted, and image contrast C_i and noise n_i were calculated as,

$$C_i = S_i - \frac{1}{N}\sum_j B_{i,j}\,, \qquad (1)$$

and

$$n_i = \sqrt{\frac{\sum_j B_{i,j} - \overline{B}_i}{N-1}}\,, \qquad (2)$$

where i is the signal sphere index, S_i is the mean pixel value for the ith signal sphere, $B_{i,j}$ is the mean pixel value for the jth background spheres (j=1-6) associated with sphere i, and N=46 is the total number of signal spheres. The ratio of C_i to n_i was used as the measure of SNR for each signal sphere, The total image SNR was the average of the individual sphere SNR's:

$$SNR = \frac{1}{N}\sum_i \frac{C_i}{n_i}\,. \qquad (3)$$

The rational for averaging the local image SNR measurements, as opposed to averaging all signal spheres and determining noise from the variations over all background spheres was to minimize the effect of any low-frequency image non-uniformity, since such non-uniformities could affect the global variations substantially while not influencing the ability to detect local lesions.

D. Optimizing LET

To optimize the 3D LET, the 3D images were reconstructed using FORE-WLS iterative algorithm, with the default image reconstruction parameters: a 4.29 mm loop filter and 3.91 mm post filter. Energy dependent calibrations such as normalization and parameters such as in the scatter model were also changed for each LET setting. Fig. 3 compares image SNR to the square root of the NEC, as a function of activity.

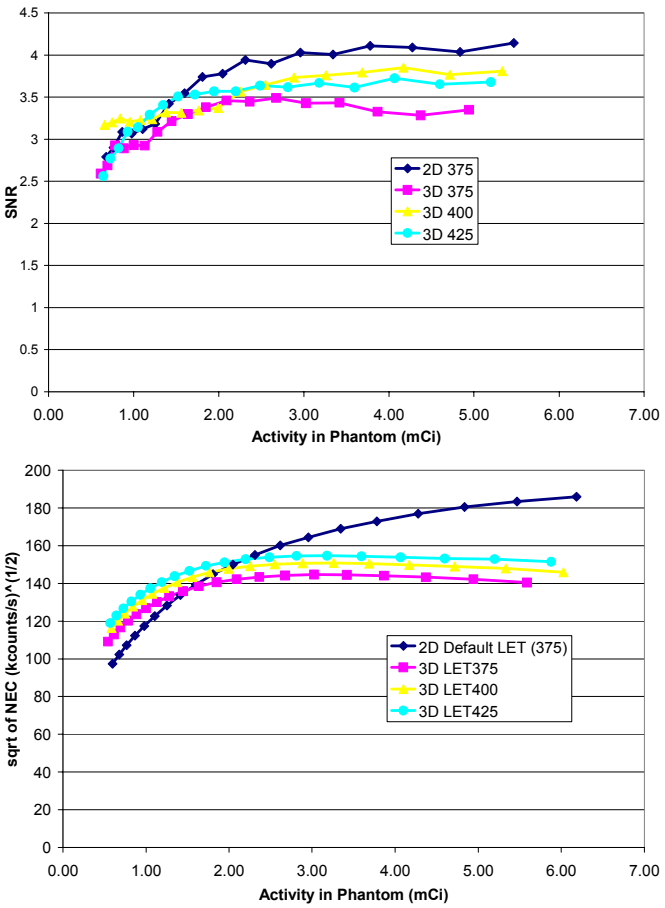

Fig. 3. SNR and square root of NEC as a function of activity.

While both the square root of NEC and the SNR show improvements of about 10% by increasing LET from its default of 375 keV, the SNR measurement are less able to distinguish between LET's of 400 and 425 keV. Based on these results, and previous line source investigations, a 3D LET of 425 keV was chosen as optimal and will be used for the remainder of this paper.

E. The effect of reconstruction algorithm.

To investigate the effects of reconstruction algorithm on image quality, 2D and 3D (LET 425 keV) images were reconstructed using a variety of algorithms, listed in Table 1 below with their associated parameters. Fig. 4 shows representative images from each reconstruction algorithm, with the CT for comparison.

TABLE 1:
IMAGE RECONSTRUCTION PARAMETERS.

Recon Type:	**Filters:**	**Subsets / Iterations.**
2D Filtered Backprojection	Hann = 7.8 mm	-
2D OS-EM	Post = 7 mm Loop = 4.3 mm	30/2
3D Reprojection	Hann = 7.8 mm Ramp = 6.5 mm	-
3D FORE-WLS	Post = 4.29 mm Loop = 3.91 mm	21/2

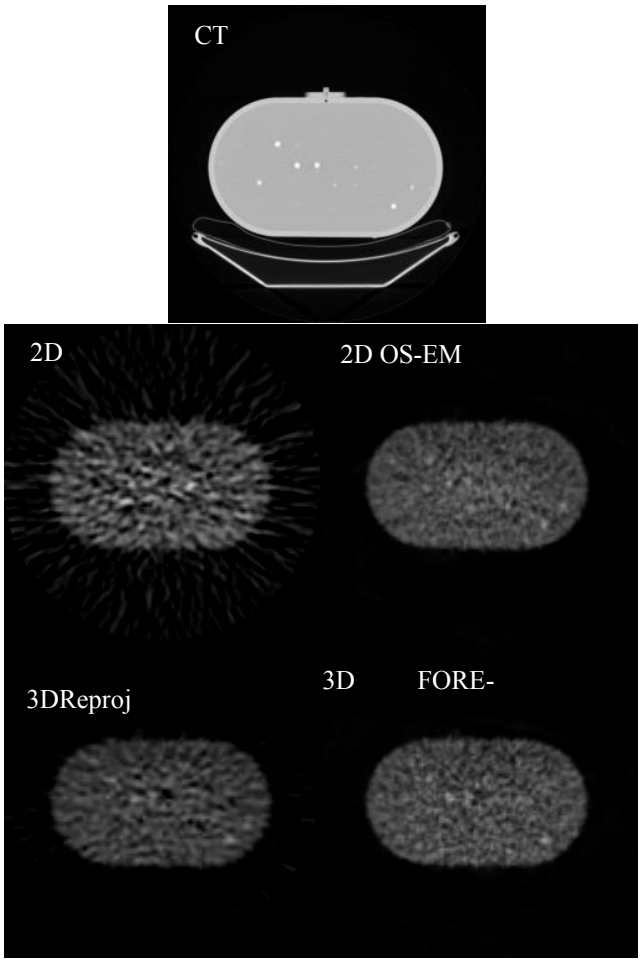

Fig. 6: Representative images for a variety of reconstruction algorithms, with the CT for comparison. From the top left: CT, 2D FBP, 2D OS-EM, 3D reprojection. 3D FORE-WLS.

For each image in the decay series, images SNR was calculated (eq. 3). Fig. 5 compares image SNR in 2D and 3D for the different reconstruction algorithms as a function of total phantom activity.

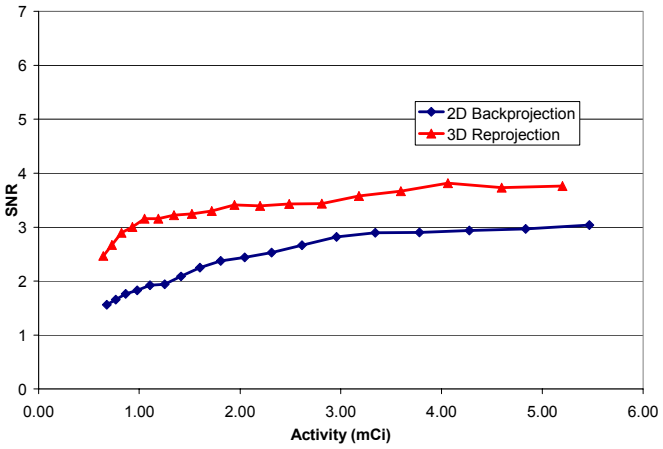

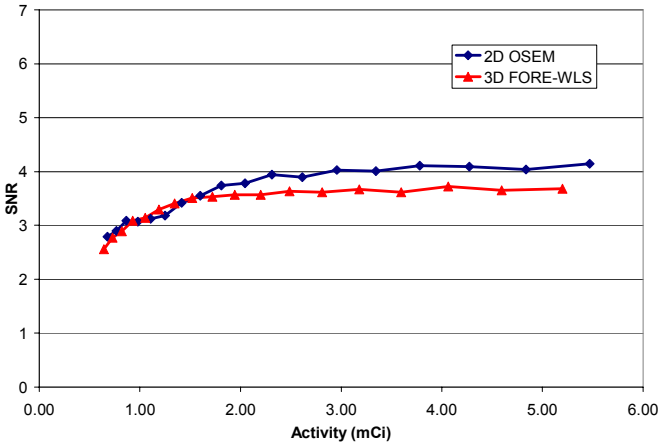

Fig. 4 SNR vs. activity in 2D and 3D for a variety of reconstruction algorithms.

Fig, 5 illustrates that the choice of reconstruction algorithm and its associated parameters can have a large effect on image quality (as measured with this way) that could not be predicted by NEC alone. The SNR curves shown in Fig. 5 are for the default system parameters, and the spatial resolutions are therefore not necessarily the same. Spatial resolution, however, is an important quantity when comparing SNR across image reconstruction algorithms. For a given reconstruction algorithm, increased post-filtering decreases the spatial resolution (and therefore the measured signal) while also decreasing the image noise. To compare reconstruction algorithms as a function of resolution, we chose one image from each decay series at an activity near the peak SNR (6.18 mCi for 2D and 3 mCi for 3D), and performed additional post-smoothing of that image using Gaussian filters of FWHM ranging from 3.2 mm to 19.2 mm. Taking the inverse of the measured signal (as derived from the phantom using eq. 1) normalized to the activity as a metric of relative image resolution, Fig. 6 shows image noise as a function of decreasing resolution for the 4 different reconstruction algorithms.

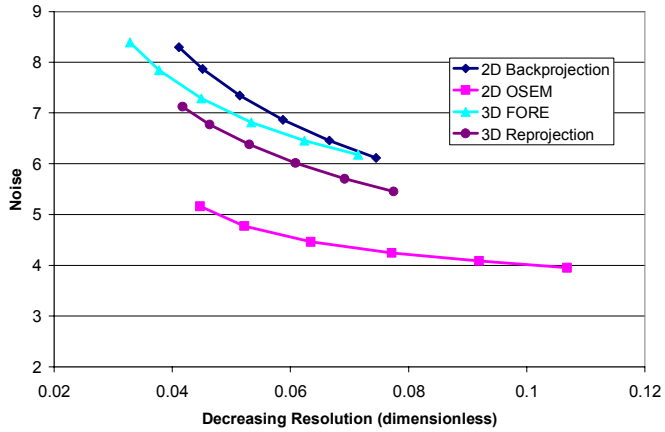

Fig. 6: Noise vs. inverse signal for a variety of reconstruction algorithms.

III. Discussion and Conclusions

The measures of image quality based on small sphere image signal-to-noise used in this study yielded different results than could have been predicted on count statistics alone. While NEC does a reasonable job of comparing the relative performance between 3D scans of different LETs, it does not account for the large difference in SNR between different image reconstruction algorithms and parameters. Furthermore, by addressing both the signal and noise components separately, our measure of SNR allows for a comparison of image noise as a function of resolution.

We find that SNR shows improved 3D performance with increased LET as predicted by line source measurements, with an LET of 425 keV being optimal. Comparing different reconstruction algorithms, we find that, for a given resolution, 2D OSEM gives the best performance in the whole body phantom, followed by 3D reprojection.

Acknowledgment

Thanks to Stephen Lokitz, Ph.D., for his assistance with the phantom measurements.

References

[1] S. C. Strother, M. E. Casey, and E. J. Hoffman. “Measuring PET scanner sensitivity: relating count rates to image signal-to-noise ratios using noise equivalent counts,” IEEE Trans. Nucl. Sci. vol. 37, no. 2, pp. 783-788, 1990.

[2] S. D. Wollenweber, K. R. Phillips, and C. W. Stearns, “Calculation of noise-equivalent image quality,” IEEE Nuclear science symposium and Medical Imaging Conference Record. vol. 4 2003.

[3] S. Pajevic, M. E. Daube-Witherspoon, S. L Bacharach, and R. E. Carson, “Noise characteristics of 3D and 2D PET images,” IEEE Trans. Med. Imaging. vol. 17, pp. 9-23, 1998.

[4] T. G. Turkington, J. W. Wilson, and J. G. Colsher. “Adjusting the low energy threshold for large bodies in PET,” Nuclear science symposium and Medical Imaging Conference Record. vol. 5 2004.

[5] J. M. Wilson, J. W. Wilson, and T. G. Turkington. “A multisphere phantom for image quality in PET/CT,” SNM 2005 conference proceedings.

[6] T. G. Turkington, N. E. Williams, S. M. Hamblen. “Regional FDG uptake, attenuation, and geometries measurements for whole body phantom design,” [abstract]. J Nucl Med. vol 40(suppl) p. 281 1999.

[7] O. Mawlawi, D. A. Podoloff, S. Kohlmyer, J. J. Williams, C. W. Stearns, R. F. Culp, and H. Macapinlac, “Performance characteristics of

a newly developed PET/CT scanner using NEMA standards in 2D and 3D Modes," J Nucl Med. vol. 45 no. 10 pp.1734-1742, October 2004.